Atomic-scale structural identification and evolution of Co-W-C ternary SWCNT catalytic nanoparticles: High-resolution STEM imaging on SiO 2

Hua An, Akihito Kumamoto, Rong Xiang, Taiki Inoue, Keigo Otsuka, Shohei Chiashi, Christophe Bichara, Annick Loiseau, Yan Li, Yuichi Ikuhara, et al.

CHEMISTRY

Atomic-scale structural identification and evolution of Co-W-C ternary SWCNT catalytic nanoparticles: High-resolution STEM imaging on SiO_2

Hua An[1], Akihito Kumamoto[2]*, Rong Xiang[1]*†, Taiki Inoue[1], Keigo Otsuka[1], Shohei Chiashi[1], Christophe Bichara[3], Annick Loiseau[4], Yan Li[1,5], Yuichi Ikuhara[2], Shigeo Maruyama[1,6†]

Recently, W-based catalysts have provided a promising route to synthesize single-walled carbon nanotubes (SWCNTs) with specific chirality, but the mechanism of the growth selectivity is vaguely understood. We propose a strategy to identify the atomic structure as well as the structure evolution of the Co-W-C ternary SWCNT catalyst. The key is to use a thin SiO_2 film as the catalyst support and observation window. As the catalyst is uniformly prepared on this SiO_2 film and directly used for the SWCNT synthesis, this method has an advantage over conventional methods: it creates an opportunity to obtain original, statistical, and dynamic understanding of the catalyst. As a technique, atomic-scale imaging directly on SiO_2 serves as a powerful and versatile tool to investigate nanocrystals and high-temperature reactions; for the synthesis of SWCNTs, this work successfully visualizes the structure and evolution of the catalyst and illuminates the possible nucleation sites of the chirality-specific growth.

INTRODUCTION

Single-walled carbon nanotubes (SWCNTs) have received considerable attention since their discovery in 1993 (*1*, *2*). This focused attention is largely driven by their one-dimensional structure and the resulting unique physical properties (*3*). One of the most interesting properties is the chirality-dependent electronic conduction, which was pioneered by M. Dresselhaus even before the observation of SWCNTs (*4*, *5*) and intensively investigated in the past decades. In brief, depending on how a graphene sheet is rolled, each SWCNT can be described as a pair of index (*n*, *m*), which uniquely determines the optical band structure of the tube. This correlation of chirality and property opens up interesting research opportunities for the community but, at the same time, brings great challenges to the controlled synthesis of SWCNT (*6*–*8*). Chirality-pure samples are needed for the large-scale application of SWCNTs in, e.g., transistors (*9*–*11*).

Recently, encouraging progress has been achieved in the chirality-controlled synthesis of SWCNTs using W-based solid catalysts. In 2014, Yang *et al.* (*12*) proposed a Co_7W_6 solid-state catalyst and achieved a chirality-selective growth of (12, 6) up to 92%. Later, we confirmed that a different Co-W-C ternary catalyst can be prepared by a simple method and maintain the selectivity at milder chemical vapor deposition (CVD) conditions (*13*). More recently, Zhang *et al.* (*14*) introduced WC and Mo_2C catalysts and obtained horizontally aligned (2*m*, *m*) SWCNTs. Although growth selectivity was demonstrated by these works, the underlying mechanism is still vaguely understood and under intensive discussion (*15*–*18*).

In all these cases, the catalyst is proven to be determinative for the successful chirality-specific growth (*19*). Identifying the structure and understanding the behavior of the catalyst therefore become indispensable. However, it has been extremely difficult to study the behavior of these nano-sized catalytic particles, especially in its original morphology. Among the available characterization techniques, transmission electron microscopy (TEM) is the most straightforward and powerful, but conventional TEM observation methods suffer from some inevitable drawbacks. For example, the information obtained could be different from the original because of compromises in the sample preparation. Even if the samples could be kept in their original forms, the information obtained in most cases is very local. In this context, TEM investigation on the catalyst structure in a reliable and atomic resolvable way becomes important for the further control over the process.

Ideally, a reliable TEM investigation on the SWCNT catalyst should meet three criteria: original (no alteration/compromise due to sample preparation), statistical (catalyst should be uniformly dispersed and the same information can be obtained everywhere), and dynamic (any catalyst change before and after the CVD, or the intermediate stages, can be identified). Here, we present a new strategy that can meet all these three criteria. The key is to use a Microelectromechanical Systems (MEMS) fabricated Si/SiO_2 grid, which allows us to perform catalyst preparation, SWCNT growth, and atomic-resolution scanning TEM (STEM) identification on the same single chip. Our Co_6W_6C catalyst is used here as an example. Its atomic structure and dynamic change have been systematically studied. The impacts of this work are as follows: (i) As a technique, the proposed TEM/STEM imaging directly on SiO_2 serves as a universal platform for studying many high-temperature catalyst behaviors and nanomaterial synthesis, and (ii) for the chirality-selective growth, this study conclusively reveals the structure as junctions of metallic W and Co_6W_6C, and the dynamic evolution process from Co_6W_6C to metallic Co is elucidated.

RESULTS

Large-area structure identification from electron diffraction

Figure 1 describes the TEM strategy proposed in this study, and the schematic structure of the chip is shown in Fig. 1 (A and B). Different from conventional Cu or Mo TEM grids, our chip has two different characteristics. First, it is fully made of Si/SiO_2 and is thermally stable up to 1000°C. Second, it is fabricated by MEMS techniques starting

[1]Department of Mechanical Engineering, University of Tokyo, Tokyo 113-8656, Japan. [2]Institute of Engineering Innovation, University of Tokyo, Tokyo 113-8656, Japan. [3]Aix-Marseille Université, CNRS, CINAM, Marseille, France. [4]Laboratoire d'Etude des Microstructures, University Paris-Saclay, CNRS-ONERA, BP72, 92322 Chatillon Cedex, France. [5]College of Chemistry and Molecular Engineering, Peking University, Beijing 100871, China. [6]Energy NanoEngineering Laboratory, National Institute of Advanced Industrial Science and Technology (AIST), Tsukuba 305-8564, Japan.
*These authors contributed equally to this work.
†Corresponding author. Email: xiangrong@photon.t.u-tokyo.ac.jp (R.X.); maruyama@photon.t.u-tokyo.ac.jp (S.M.)

from a silicon wafer. These two characteristics allow one to perform catalyst preparation and SWCNT growth in the exact same way as a conventional substrate. Therefore, the concept is to use this Si/SiO_2 TEM chip to perform a transfer-free and uncompromised characterization of the catalysts in their real morphologies: the same catalyst and supporting substrate as the conventional CVD.

A thin, suspended SiO_2 film serves as the observation window in our structure (Fig. 1B). The first technical challenge for this window is that SiO_2 is an electron insulator. TEM imaging through this SiO_2 becomes unstable at a conventionally high electron dose because of electron accumulation (usually recognized as charge-up effect). We performed an estimate of the charge density on this SiO_2 window, which is shown in Fig. 1C (calculation details shown in fig. S2). Briefly, the results suggest that at the same beam condition, the accumulated charge density at the edge and particularly at the corner of this SiO_2 film is less than 10% of the value when the beam is placed at the center. Therefore, we perform most of the current study using the corner of the window. In the experiment, decently high currents can be applied without bringing significant charge-up during the TEM and STEM observations.

The catalyst studied in this work is a Co-W-C ternary system, which is able to produce (12, 6) dominant SWCNTs at a relatively mild condition. The unintentional incorporation of C into the catalyst during

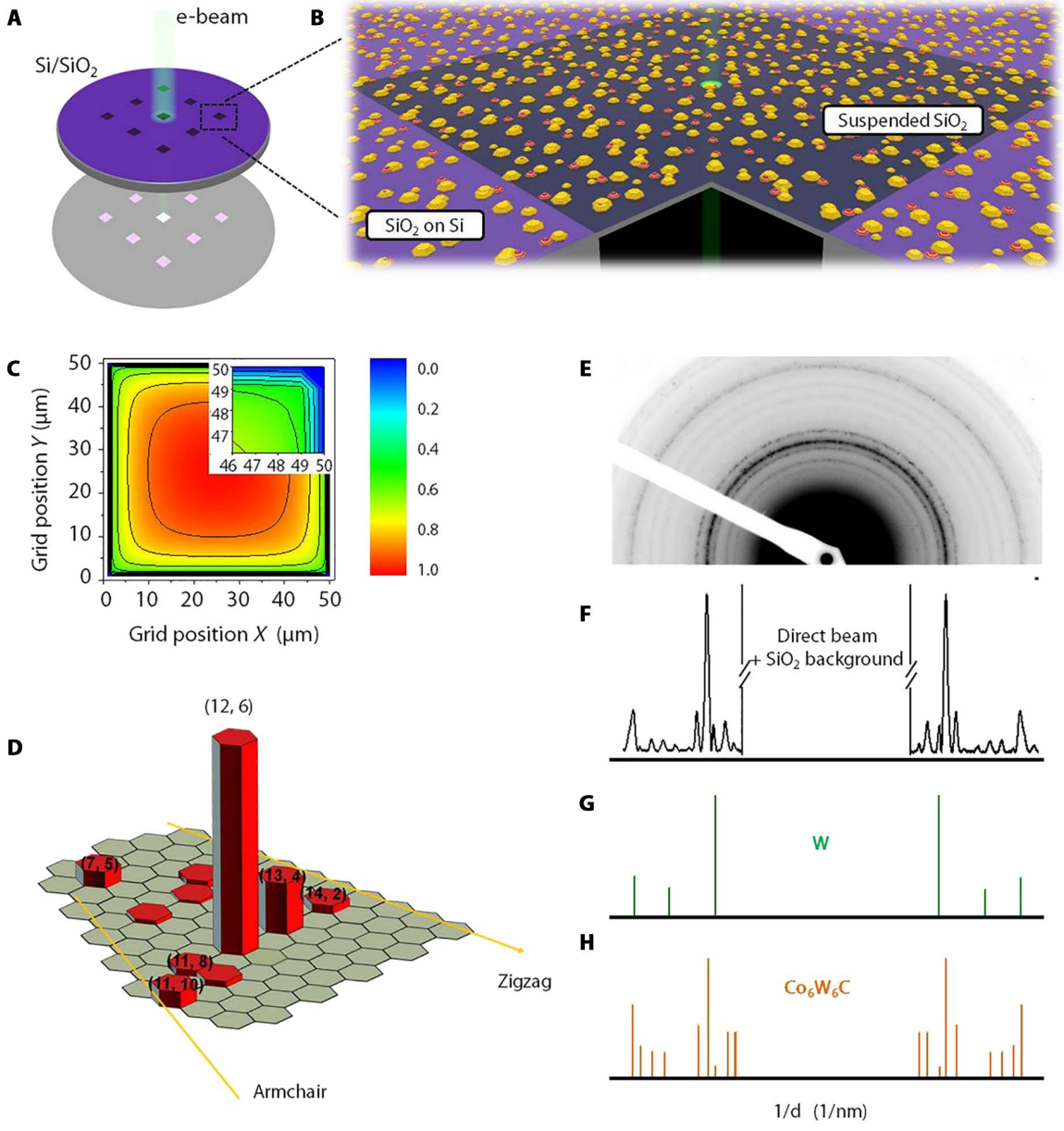

Fig. 1. Overview of the proposed TEM method, produced SWCNTs, and the structure of the catalyst. (**A**) Schematic of the 3-mm-diameter Si/SiO_2 TEM grid. (**B**) The enlarged schematic showing a 20-nm-thin suspended SiO_2 serves as the TEM observation window, and the catalyst can be prepared directly on this film and dispersed uniformly. (**C**) Estimated distribution of charge density over the suspended SiO_2 film, suggesting that electron accumulation at edges and corners of the window is less than 10% of the value in the center. (**D**) Chirality distribution of SWCNTs synthesized from the Co-W-C catalyst. (**E**) Typical SAED pattern of the reduced Co-W-C catalyst. (**F**) Intensity profile of SAED pattern in (E). (**G** and **H**) Standard powder diffraction file of metallic W (no. 04-0806) and Co_6W_6C (no. 23-0939).

reduction resulted in the formation of this carbon-containing ternary catalyst, as has been discussed in our previous report (*13*). The chirality distribution of the produced SWCNTs is plotted in Fig. 1D. This chirality analysis is performed on a conventional Si/SiO_2 substrate, but a comparison of SWCNTs on the TEM chip with the conventional cases on standard Si/SiO_2 substrates is shown in fig. S1, where the scanning electron microscopy (SEM) images and Raman spectroscopy suggest that SWCNTs are similar. The dominant peak in Raman spectra comes from (12, 6) SWCNT, while some other peaks also appear at much lower intensity. The enrichment of (12, 6) SWCNT is 50 to 70%, as estimated from Raman spectroscopy and cross-checked by optical absorption spectroscopy. More details on the characterization on these SWCNTs can be found in our previous report (*13*). Figure 1E shows a typical selected-area electron diffraction (SAED) pattern of our Co-W-C catalyst prepared by sputtering. The selective area aperture used is several micrometers in diameter, meaning the SAED pattern contains information from more than 10,000 particles. This is the first strength for the current technique: Very statistical data are obtained. The intensity profile is plotted in Fig. 1F. After comparing it with the standard powder diffraction file (PDF no. 04-0806 and PDF no. 23-0939; Fig. 1, G and H), we conclude that our catalyst contains two main phases: a body-centered cubic (bcc) metallic W phase and an η carbide Co_6W_6C phase. Gaining this large-area statistical information is nearly impossible if the catalyst is not uniformly and flatly dispersed. On our grid, the same results are obtained everywhere on the SiO_2 window. However, one should also note that SAED patterns only reveal crystal phases; the amorphous compound or poorly crystallized particles, if existing, are less pronounced because they have weak diffractions. Furthermore, there is no information about how such two crystals distribute on the surface. They may stay separately or form joint particles with crystal interfaces. To distinguish these, higher-resolution STEM is used here to directly image the crystal phases and their interfaces and to distinguish whether any less-crystallized phases exist, all of which we could not answer by conventional TEM in our previous study (*13*).

Single-particle structure identification from direct STEM imaging

Figure 2 presents the energy-dispersive x-ray spectroscopy (EDS) and direct STEM imaging at the single-particle level. Together with the SAED patterns in the previous section, the geometry and structure of the catalyst can be fully illustrated. These images are taken at room temperature, but similar phases are confirmed by SAED when the sample is heated to higher temperatures in TEM. The EDS mappings shown in Fig. 2 (A to C) present the elemental distribution of Co and W on the suspended SiO_2 film. Two types of particles can be identified from this map. The type I particles are yellow, which suggests that they are pure W. The type II particles are junctions of a yellow segment (pure W) and a pinkish section. This pinkish segment is a mixture of Co and W, as compared in Fig. 2 (B and C). In this section, we used a new atomic counting EDS technique, which gives the quantitative ratio between atoms. This analysis suggests that the overall atomic ratio is 71:29, meaning W is excessive for forming Co_6W_6C. This excess of W makes Co react with W entirely after reduction and explains why no pure pink phase (pure Co) is observed. We believe that the absence of pure Co is critical for the successful growth of selective chirality, because pure Co is known to be very efficient for the growth of SWCNTs with various chiralities.

More detailed structure of the junctions can be revealed by direct STEM imaging. The bottom part of Fig. 2E suggests that this is a metallic bcc W phase viewing from the [111] direction, which corresponds to the purely yellow phase in the EDS mapping. The top part, however, is a mixture of Co and W with a more complicated crystal structure. We tilted the sample to get a zone axis of this crystal domain, and the high-angle annular dark-field (HAADF) and annular bright-field (ABF) images are shown in Fig. 2 (F and G). According to the SAED patterns in Fig. 1, it is very likely to be the Co_6W_6C phase. Co_6W_6C, known as η carbide, has a quite complicated cubic structure, which consists of eight regular octahedra of tungsten atoms centered in a diamond cubic lattice and eight regular tetrahedra of Co atoms centered in the second diamond cubic lattice (*20*). The unit cell is as long as 1 nm in each direction. To solidify the identification from SAED patterns, we simulated the STEM images of Co_6W_6C at different crystal directions. The comparison between experimental and simulated images in Fig. 2H gives a reliable matching and confirms that the crystal is the [310] zone axis of Co_6W_6C. The particles studied here are typically 4 to 10 nm. Although it may be generally speculated that smaller-diameter particles (e.g., ~1 nm) are more active and responsible for the SWCNT growth, very small particles can be hardly found in the current catalyst. The data shown here are fairly representative; similar images can be obtained everywhere on the SiO_2 window, as the particles are uniformly dispersed over the surface.

Further analysis suggests that there is no clear crystal orientation relationship between Co_6W_6C and W after checking more particles. We emphasize this point because a different case is observed in the later part of this study (to be shown later). This absence of a clear crystal orientation relationship is understandable because these two phases both have very high melting temperatures and were possibly formed independently during the reduction process before aggregating into a junction. Nonetheless, we believe that the geometry and structure of our catalyst are conclusive after this STEM imaging. The catalyst contains no noticeable amorphous phase but only two types of particles: (i) bcc metallic W and (ii) junctions of W-Co_6W_6C. Some previous attempts use SiO_2 spheres, the edge of a carbon TEM grid as the catalyst support, or conventional slicing techniques to visualize the catalyst (*21*, *22*). However, the current study demonstrates that it is possible to obtain atomic-resolution analysis on a flat and continuous thin SiO_2 film even for a very complicated ternary structured catalyst. This high resolution serves as the second strength of our approach. This is also the first direct imaging of the η-Co_6W_6C structure.

Dynamic evolution of Co-W-C structure with atomic resolution

The thin SiO_2 film is thermally stable at high temperatures up to 1000°C; therefore, CVD can be performed on our TEM chip. The compatibility to the CVD, which serves as the third strength of this technique, opens up a new possibility for studies that were previously impossible. The evolution of the catalyst (e.g., size change aggregation and phase change) during the reaction can be resolved. Figure 3 presents EDS mapping and the typical spectra of the reduced, 1-min CVD reacted, and 3-min CVD reacted Co-W-C catalyst (SEM images and Raman spectra of the corresponding samples are shown in fig. S3). We found that the Co-W-C catalyst particles encounter a change in morphology after exposure to the carbon source. This loss of W is unexpected, as catalyst-like WC was found to be very stable (*23*), but it becomes possible when oxygen in ethanol interacts with W via oxide or hydroxide (*13*). From the EDS analysis in Fig. 3B, one can see a significant decrease in the relative intensity of W even after a 1-min CVD. As previously noted, the current EDS can quantitatively analyze the atoms in this area;

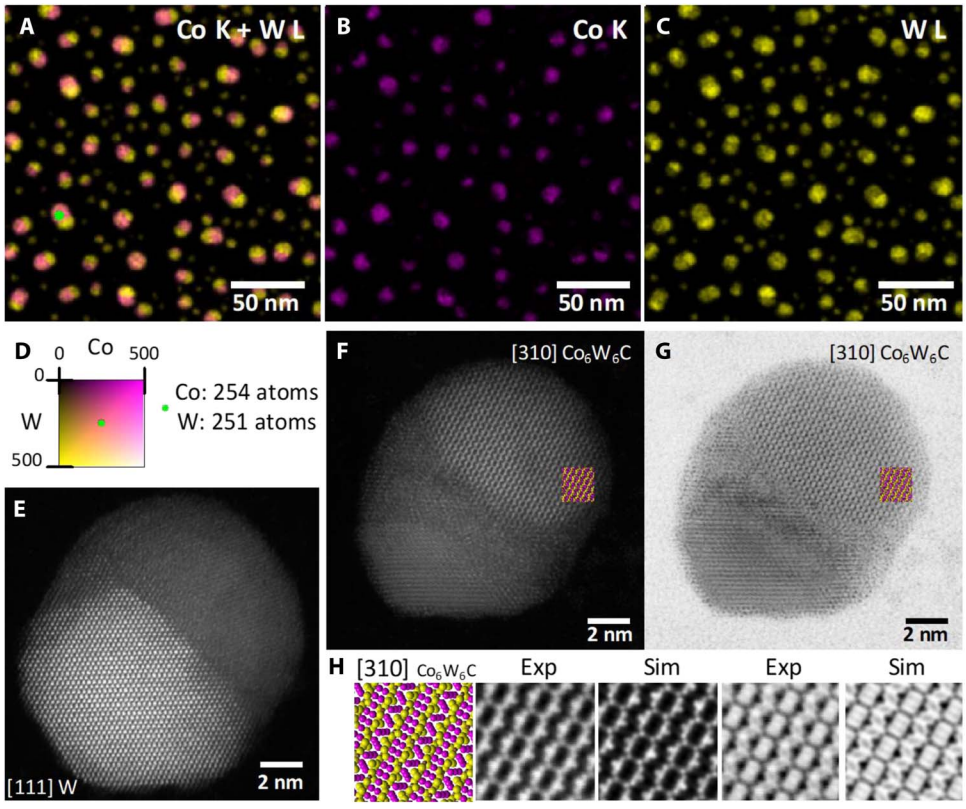

Fig. 2. Atomic structure identification of Co-W-C. (**A** to **D**) Quantitative EDS mapping of the reduced Co-W-C catalyst on the suspended SiO_2 film, suggesting that two types of particles are existing: (i) pure W and (ii) junctions of pure W and Co-W mixtures. (**E**) HAADF image of a junction particle viewed from the [111] direction of the bottom part, suggesting that it is a metallic bcc W phase. (**F**) HAADF- and (**G**) ABF-STEM image of the same particle tilted to the [310] axis of the upper half of the particle, suggesting a Co_6W_6C phase. (**H**) Structure model and comparison of experimental and simulated HAADF- and ABF-STEM images of Co_6W_6C from the direction of [310].

therefore, the decrease of the W signal suggests that W gradually disappears during the CVD. SAED patterns of the catalyst after different CVD durations reveal the same trend (fig. S4). The relative W/Co atomic ratio decreases from 71:29 (original) to 41:59 (3-min growth).

Typical atomic structures of the 1-min and 3-min CVD reacted catalyst are shown in Fig. 4. In both samples, the Co_6W_6C phase persists, as can be confirmed by the experimental and simulated STEM images. However, the W phase shows a clear difference. In the former case, the pure W segment (the bottom of the image) becomes a W-enriched W-Co mixture according to EDS quantitative analysis. This W-dominant part still exists, but the size becomes much smaller than the original shape (0 min). In the latter case, after a 3-min CVD, W-enriched phases are hardly observable and typical particles (Fig. 4, D and E) contain only a single Co_6W_6C phase. This is probably because loss of W starts from this pure W phase, and the Co_6W_6C structure is more stable than pure W in our growth environment.

In the 3-min CVD–reacted catalyst, precipitation of Co phases is observed. Figure 5 (A to E) shows a representative particle with a junction structure. This particle is imaged from the [111] zone axis of the Co_6W_6C crystal, and experimental results match perfectly with the image simulated from the atomic model, as shown in Fig. 5F. However, different from the junctions in the as-reduced catalyst, the current junction contains a Co_6W_6C phase and a pure Co (pink) phase. It is probably formed when the amount of W further decreases as CVD proceeds, and Co finally becomes oversaturated in a Co-W particle. The atom-resolved STEM images show that the pure Co phase has a hexagonal close-packed (hcp) structure, and more significantly, the precipitation of Co is fully coherent to the parent Co_6W_6C structure. A coherent precipitation means that two crystals have strict crystallographic relationship, which, in the current case, can be described as [$11\bar{2}0$] hcp-Co // [111] Co_6W_6C and [0001] hcp-Co // [$1\bar{1}0$] Co_6W_6C, while the interface inclined from the planes of (0001) hcp-Co and ($1\bar{1}0$) Co_6W_6C. Figure S5 shows images of another particle in the same sample. The trend is similar to the previous particle, but the concentration of W is even lower. The precipitation of hcp Co is in contrast to those of previous reports (*24*–*26*), where SWCNTs nucleate from cobalt carbide and face-centered cubic (fcc) Co. This difference is reasonable because a parent crystal exists in the current case and acts as a template for the precipitation of Co. From both SAED and direct imaging, no noticeable pure cobalt carbide is evidenced in our catalyst. Phase separation in the bimetallic SWCNT catalyst was speculated in previous studies but had not been satisfactorily evidenced. For example, x-ray photoelectron spectroscopy suggested that in the Co-Mo catalyst, the metallic Co phase coexisted with molybdenum carbide after reduction (*22*, *27*). It is not until recently that developments in TEM/STEM have allowed access to the detailed structure of an individual particle. In one case, Fe-Pt was found to form a junction of Fe and FePt alloy (*28*), while in another case, Co-Cu stayed as two separate phases without forming an alloy or a compound (*29*). The current study further extends our understandings on

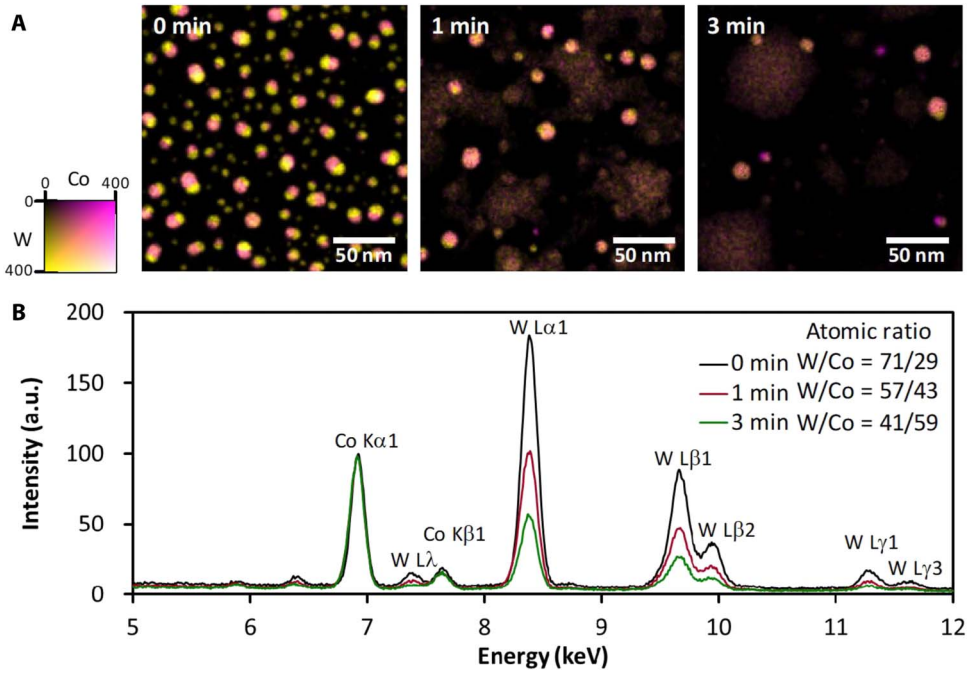

Fig. 3. Elemental evolution of Co-W-C after different CVD time. (**A**) Quantitative EDS mappings of reduced and reacted Co-W-C catalyst particles on Si/SiO_2 grids. (**B**) Typical EDS spectra of different samples, showing a clear decrease of atomic ratio of W/Co along with CVD. a.u., arbitrary units.

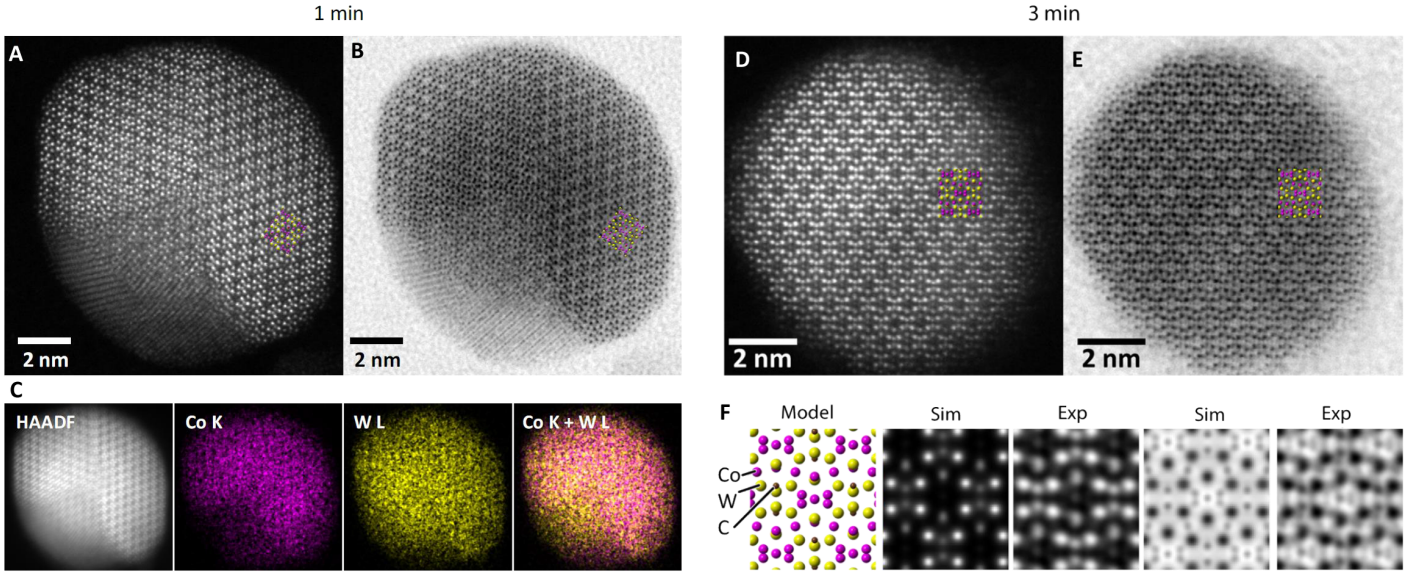

Fig. 4. Structure evolution of Co-W-C during CVD. (**A**) HAADF- and (**B**) ABF-STEM images and (**C**) EDS mapping of the reacted Co-W-C catalyst after a 1-min CVD, showing that the particle is a junction of the W-enriched phase and Co_6W_6C, but the W-enriched phase is much smaller than the pure W phase in the reduced catalyst. (**D**) HAADF- and (**E**) ABF-STEM images and (**F**) structure model and comparison of simulated and experimental STEM images of the reacted Co-W-C catalyst after a 3-min CVD, showing that this particle contains only the Co_6W_6C phase and W-enriched phases disappeared after a 3-min CVD.

the SWCNT catalyst, with both the incoherent W-Co_6W_6C and coherent Co_6W_6C-Co atomically illustrated. To this end, we have obtained a clear picture of the evolution that happened on the Co-W catalyst during the entire CVD process.

We summarize the overall process observed so far, with a ternary Co-W-C phase diagram shown in Fig. 5G as a reference (*30*). Although a bulk phase diagram does not explain the particle behavior or crystal interface at the nanoscale, it helps to roughly understand the phase change and candidate structure. The reduced catalyst started from the position in the diagram identified with a red asterisk. After reduction, W is excessive, so most particles segregate into two stable compounds with fixed composition (note: not an alloy in our Co-W-C case). At this stage,

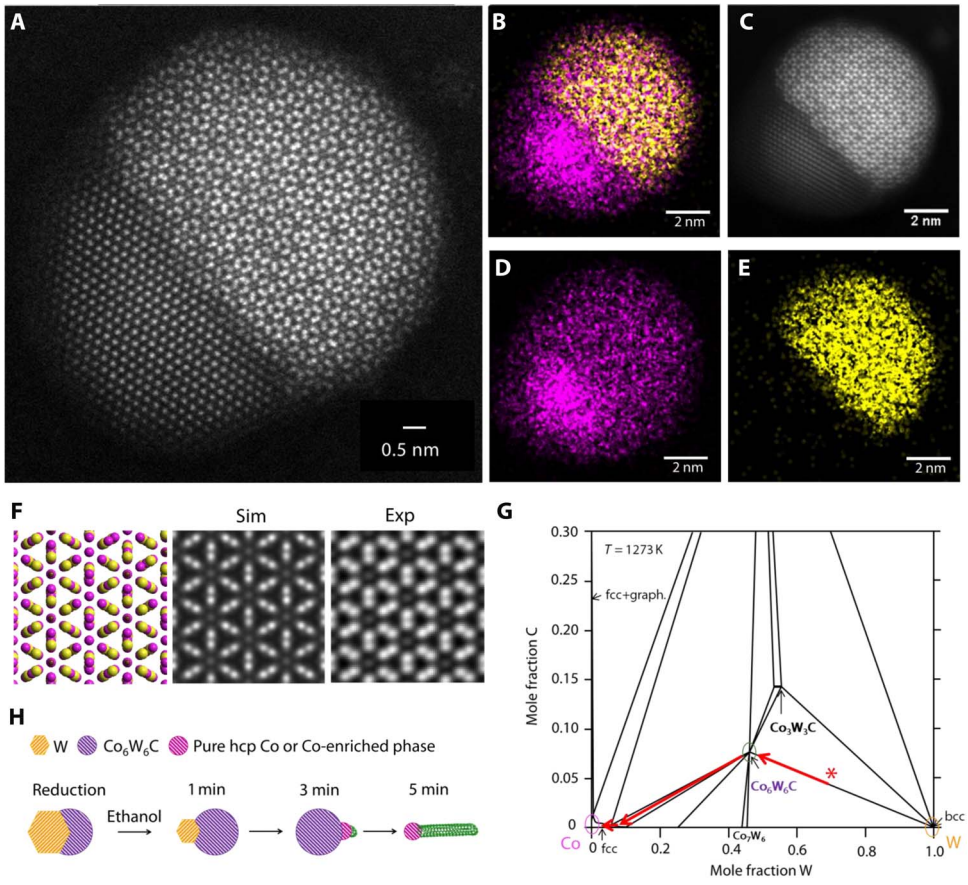

Fig. 5. Precipitation of Co and Co-enriched phase. (**A**) Atomic-resolution HAADF-STEM image of a 3-min reacted Co-W-C catalyst particle, showing that the particle is a junction of the Co_6W_6C and pure Co phase. (**B** to **E**) EDS mapping of the same particle (pink represents Co K and yellow represents W L) and HAADF-STEM image taken simultaneously during EDS mapping. (**F**) Comparison between simulated and experimental STEM image of Co_6W_6C. These results suggest an oversaturation and precipitation of Co or Co-enriched phase from Co_6W_6C when the CVD time is extended. (**G**) Bulk phase diagram of Co-W-C ternary system remade from (*30*). (**H**) Schematic showing the overall process revealed in this work and a possible nucleation mechanism of SWCNTs (pink and yellow).

the Co-W-C catalyst underwent long reduction and therefore reached a thermodynamically-stable two phases. However, upon the introduction of the carbon source, the W concentration on the surface quickly decreases, and the composition moves to the left part of the diagram. In this part, the thermodynamically stable phases are Co_6W_6C and pure Co. The details of each particle and the relationship of the crystal phase can be obtained by our STEM images of each particle, which shows that the precipitated Co is fully coherent to Co_6W_6C. Overall, the conclusion for our Co-W-C catalyst is that metallic W is unstable in the CVD but Co_6W_6C can survive for a relatively long time during the CVD. Last, we make a simple scheme showing the evolution of the Co-W-C catalyst (Fig. 5H). The SWCNT is drawn for eye guide only, and it is likely, but we do not claim, that SWCNTs are formed directly from a certain-phase.

However, the findings of this study suggest three possible factors that could contribute to the chirality-selective growth of SWCNTs. First and most likely, SWCNTs nucleate and precipitate from a certain facet of the Co_6W_6C crystal. As this ternary crystal has a complicated structure, energy matching for an SWCNT on different facets can be different, as has been discussed and predicted in the case of Co_7W_6 (*12*). A second possibility is the role of interface. Along with the loss of W atoms in a Co_6W_6C particle, oversaturated C can possibly precipitate, particularly at the interface of Co and Co_6W_6C (*6*, *31*). As steps are observed in the reacted catalyst, how much crystal steps contributed to structure selectivity was argued before but is still not fully concluded. Last, although less likely, the possibility of growth from the pure Co phase cannot be ruled out. Because of the coherent precipitation, certain facets of hcp Co may predominately appear during the CVD and promote the formation of (12, 6) SWCNTs. We highlight the second and third mechanisms, i.e., the role of crystal change, on the chirality-selective growth particularly after we realize that the SWCNT growth is not occurring immediately after the introduction of the carbon source. It usually takes more than 30 s before we can observe the growth of SWCNTs from SEM or detect the signal of (12, 6) SWCNTs from Raman (fig. S3). Therefore, it is possible that the nucleation of (12, 6) SWCNT started during the dynamic evolution of our catalyst. Fully clarifying the secrets of chirality selectivity requires a simultaneous imaging of the nanotube and catalyst on SiO_2 in a statistical manner. Although it is still not yet possible in the current study to answer from which sites SWCNTs are formed, the methodology established here has proven its capability of identifying the structure and behavior of the complicated catalyst. With illustrated crystal structure and evolution pathways, we believe that we have taken a significant step toward revealing the mechanism behind the chirality selectivity. In addition, this method may be applied to other catalysts and high-temperature reactions.

DISCUSSION

We proposed a TEM method that is able to identify the structure as well as the structure evolution of Co-W-C ternary catalytic nanoparticles during the chirality-selective synthesis of SWCNTs. The key was to use a MEMS-fabricated SiO_2 film that is thick enough to serve as the catalyst support but thin enough to serve as the observation window. We demonstrated that atomic-resolution STEM images can be obtained directly on the SiO_2 film. The Co-W-C ternary catalyst is confirmed to be junctions of W and Co_6W_6C after reduction. However, a significant loss of W is observed by quantitative EDS after the CVD starts, and last, hcp Co is precipitated coherently from the parent Co_6W_6C crystal. Growing SWCNTs could also be possible on other types of commercial or home-modified grids, e.g., Si_4N_3 TEM grid or SiO_2-coated metal/carbon grids. But only the current Si/SiO_2 grid gives, as far as we understand, a nearly (if not exactly) identical environment to the conventional growth on the Si/SiO_2 substrate. It is also advantageous in terms of being able to obtain a large-area uniformity, to minimize the possible difference in the quality of SiO_2, and to eliminate the effect of metallic impurities.

One remaining problem in this work is that C is not visible in HAADF images. Although potentially this method could identify a catalyst-SWCNT junction, imaging them simultaneously on the SiO_2 film is still not easy. Therefore, we are unable to conclude from direct imaging at which stage SWCNTs begin to appear or from which phase direction SWCNTs nucleate. However, as a next step, we might be able to image an SWCNT in the TEM mode and switch to STEM to resolve the atomic structure. Similarly, we noticed that the SWCNTs grown by this catalyst are usually curled. It is not impossible that kinks form and change the chirality along one SWCNT. Therefore, being able to grow straight SWCNTs may be crucial for improving chirality enrichment in our samples. Nonetheless, we believe that the method proposed here opens up new possibilities for studying nano-sized particle behavior in their original morphologies and in a statistical manner. In particular, the dynamic change before and after high-temperature reactions becomes possible. More applications, which include but are not limited to SWCNT growth, are expected in the future.

MATERIALS AND METHODS

Synthesis of SWCNTs

(12, 6)-enriched SWCNTs were grown by alcohol catalytic CVD method using the bimetallic Co-W catalyst prepared by sputtering. Briefly, 0.7-nm W and 0.3-nm Co were sputtered (using C-400-2C-APD-1S, ULVAC Riko) on the Si/SiO_2 wafer substrate with an oxide layer of 300 nm. The substrates were then transferred into a tube furnace and heated in Ar/H_2 (3% H_2) at a pressure of 40 kPa, followed by a reduction at 850°C for 5 min. Then, the furnace temperature was reduced to 750°C, and the growth was conducted at 750°C at a low-pressure CVD with ethanol as the carbon source (1.3 kPa) for the controlled target growth time. After the CVD, ethanol flow was closed and the catalyst was cooled down to room temperature in a flow of 300 sccm (standard cubic centimeters per minute) Ar/H_2 (3% H_2). To study the structure and evolution of the catalyst, a similar process was carried out on a Si/SiO_2 TEM grid.

Characterization of SWCNTs

The as-grown SWCNT samples were characterized by an SEM (Hitachi S-4800) at an accelerating voltage of 1 kV and using a Raman spectrometer (inVia, Renishaw) with excitation wavelengths of 488, 532, 633, and 785 nm. Raman mapping was performed to obtain more quantitative results about the SWCNT content. Because the spot size of the laser was smaller than 2 μm and the SWCNT length was approximately 2 to 5 μm, as obtained from SEM characterization, an 8-μm spacing was used to avoid the overcounting of the same SWCNT. The equation $\omega_{RBM} = 235.9/d_t + 5.5$ was used to calculate the diameter of SWCNT, and (n, m) assignment was performed according to the method previously proposed (*32*).

TEM/STEM imaging of catalyst

The low-magnification TEM images were obtained by conventional TEMs operated at 200 kV (JEM-2000EX and JEM-2010F, JEOL Co. Ltd.). SAED patterns were obtained using a charge-coupled device camera or a negative film. A typical camera length was 60 cm, and the exposure time was from 2 to 30 s. Because the diffraction rings of W are very clear, we precisely calibrated the camera length and made the other diffraction rings to determine Co_6W_6C, but not Co_3W_3C, which has a very similar pattern except for the lattice parameter. HAADF-STEM, ABF-STEM, and EDS were obtained by probe-forming aberration-corrected STEM (200 kV, JEM-ARM200F Cold-FEG dual SDD, JEOL Co. Ltd.).

STEM image simulation

STEM image simulations of Co_6W_6C were performed using commercially available and accelerated multislice simulation software (elbis, BioNet Laboratory Inc.) (*33*, *34*). The microscopic parameters in the simulation were set to an accelerating voltage of 200 kV, an aberration-free probe with a semiconvergence angle of 22 mrad, and a specimen thickness of 6 to 10 nm.

SUPPLEMENTARY MATERIALS

Supplementary material for this article is available at http://advances.sciencemag.org/cgi/content/full/5/5/eaat9459/DC1

Supplementary Materials and Methods

Fig. S1. Comparison of SWCNTs grown on Si/SiO_2 substrate and Si/SiO_2 TEM grid.

Fig. S2. Details of the relative surface charge estimation.

Fig. S3. SEM images and Raman spectra of the SWCNTs.

Fig. S4. Low-magnification TEM and SAED patterns of the Co-W catalyst.

Fig. S5. STEM images of another reacted Co-W-C particle with a less W concentration.

REFERENCES AND NOTES

1. S. Iijima, T. Ichihashi, Single-shell carbon nanotubes of 1-nm diameter. *Nature* **363**, 603–605 (1993).
2. D. S. Bethune, C. H. Kiang, M. S. de Vries, G. Gorman, R. Savoy, J. Vazquez, R. Beyers, Cobalt-catalyzed growth of carbon nanotubes with single-atomic-layerwalls. *Nature* **363**, 605–607 (1993).
3. R. Saito, G. Dresselhaus, M. S. Dresselhaus, *Physical Properties of Carbon Nanotubes* (World Scientific, 1998).
4. R. Saito, M. Fujita, G. Dresselhaus, M. S. Dresselhaus, Electronic-structure of chiral graphene tubules. *Appl. Phys. Lett.* **60**, 2204–2206 (1992).
5. M. S. Dresselhaus, G. Dresselhaus, R. Saito, C60-related tubules. *Solid State Commun.* **84**, 201–205 (1992).
6. M. S. He, H. Jiang, B. Liu, P. V. Fedotov, A. I. Chernov, E. D. Obraztsova, F. Cavalca, J. B. Wagner, T. W. Hansen, I. V. Anoshkin, E. A. Obraztsova, A. V. Belkin, E. Sairanen, A. G. Nasibulin, J. Lehtonen, E. I. Kauppinen, Chiral-selective growth of single-walled carbon nanotubes on lattice-mismatched epitaxial cobalt nanoparticles. *Sci. Rep.* **3**, 1460 (2013).
7. B. Liu, F. Wu, H. Gui, M. Zheng, C. Zhou, Chirality-controlled synthesis and applications of single-wall carbon nanotubes. *ACS Nano* **11**, 31–53 (2017).
8. H. Wang, L. Wei, F. Ren, Q. Wang, L. D. Pfefferle, G. L. Haller, Y. Chen, Chiral-selective $CoSO_4/SiO_2$ catalyst for (9,8) single-walled carbon nanotube growth. *ACS Nano* **7**, 614–626 (2013).
9. M. M. Shulaker, G. Hills, N. Patil, H. Wei, H.-Y. Chen, H.-S. P. Wong, S. Mitra, Carbon nanotube computer. *Nature* **501**, 526–530 (2013).

10. C. G. Qiu, Z. Zhang, M. Xiao, Y. Yang, D. Zhong, L.-M. Peng, Scaling carbon nanotube complementary transistors to 5-nm gate lengths. *Science* **355**, 271–276 (2017).
11. A. D. Franklin, The road to carbon nanotube transistors. *Nature* **498**, 443–444 (2013).
12. F. Yang, X. Wang, D. Zhang, J. Yang, D. Luo, Z. Xu, J. Wei, J.-Q. Wang, Z. Xu, F. Peng, X. Li, R. Li, Y. Li, M. Li, X. Bai, F. Ding, Y. Li, Chirality-specific growth of single-walled carbon nanotubes on solid alloy catalysts. *Nature* **510**, 522–524 (2014).
13. H. An, A. Kumamoto, H. Takezaki, S. Ohyama, Y. Qian, T. Inoue, Y. Ikuhara, S. Chiashi, R. Xiang, S. Maruyama, Chirality specific and spatially uniform synthesis of single-walled carbon nanotubes from a sputtered Co-W bimetallic catalyst. *Nanoscale* **8**, 14523–14529 (2016).
14. S. C. Zhang, L. Kang, X. Wang, L. Tong, L. Yang, Z. Wang, K. Qi, S. Deng, Q. Li, X. Bai, F. Ding, J. Zhang, Arrays of horizontal carbon nanotubes of controlled chirality grown using designed catalysts. *Nature* **543**, 234–238 (2017).
15. N. Pierce, G. Chen, L. P. Rajukumar, N. H. Chou, A. L. Koh, R. Sinclair, S. Maruyama, M. Terrones, A. R. Harutyunyan, Intrinsic chirality origination in carbon nanotubes. *ACS Nano* **11**, 9941–9949 (2017).
16. F. Ding, A. R. Harutyunyan, B. I. Yakobson, Dislocation theory of chirality-controlled nanotube growth. *Proc. Natl. Acad. Sci. U.S.A.* **106**, 2506–2509 (2009).
17. S. Reich, L. Li, J. Robertson, Control the chirality of carbon nanotubes by epitaxial growth. *Chem. Phys. Lett.* **421**, 469–472 (2006).
18. F. Zhang, P.-X. Hou, C. Liu, H.-M. Cheng, Epitaxial growth of single-wall carbon nanotubes. *Carbon* **102**, 181–197 (2016).
19. H. Wang, Y. Yuan, L. Wei, K. Goh, D. Yu, Y. Chen, Catalysts for chirality selective synthesis of single-walled carbon nanotubes. *Carbon* **81**, 1–19 (2015).
20. D. V. Suetin, I. R. Shein, A. L. Ivanovskii, Structural, electronic and magnetic properties of eta carbides (Fe_3W_3C, Fe_6W_6C, Co_3W_3C and Co_6W_6C) from first principles calculations. *Physica B* **404**, 3544–3549 (2009).
21. H. W. Zhu, K. Suenaga, A. Hashimoto, K. Urita, K. Hata, S. Iijima, Atomic-resolution imaging of the nucleation points of single-walled carbon nanotubes. *Small* **1**, 1180–1183 (2005).
22. M. Hu, Y. Murakami, M. Ogura, S. Maruyama, T. Okubo, Morphology and chemical state of Co-Mo catalysts for growth of single-walled carbon nanotubes vertically aligned on quartz substrates. *J. Catal.* **225**, 230–239 (2004).
23. D. N. Yuan, L. Ding, H. Chu, Y. Feng, T. P. McNicholas, J. Liu, Horizontally aligned single-walled carbon nanotube on quartz from a large variety of metal catalysts. *Nano Lett.* **8**, 2576–2579 (2008).
24. M. Picher, P. A. Lin, J. L. Gomez-Ballesteros, P. B. Balbuena, R. Sharma, Nucleation of graphene and its conversion to single-walled carbon nanotubes. *Nano Lett.* **14**, 6104–6108 (2014).
25. L. L. Zhang, M. He, T. W. Hansen, J. Kling, H. Jiang, E. I. Kauppinen, A. Loiseau, J. B. Wagner, Growth termination and multiple nucleation of single-wall carbon nanotubes evidenced by in situ transmission electron microscopy. *ACS Nano* **11**, 4483–4493 (2017).
26. Y. Qian, H. An, T. Inoue, S. Chiashi, R. Xiang, S. Maruyama, A comparison between reduced and intentionally oxidized metal catalysts for growth of single-walled carbon nanotubes. *Phys. Status Solidi B* **255**, 1800187 (2018).
27. D. E. Resasco, W. E. Alvarez, F. Pompeo, L. Balzano, J. E. Herrera, B. Kitiyanan, A. Borgna, A scalable process for production of single-walled carbon nanotubes (SWNTs) by catalytic disproportionation of CO on a solid catalyst. *J. Nanopart. Res.* **4**, 131–136 (2002).
28. M. He, H. Jin, L. Zhang, H. Jiang, T. Yang, H. Cui, F. Fossard, J. B. Wagner, M. Karppinen, E. I. Kauppinen, A. Loiseau, Environmental transmission electron microscopy investigations of Pt-Fe_2O_3 nanoparticles for nucleating carbon nanotubes. *Carbon* **110**, 243–248 (2016).
29. K. H. Cui, A. Kumamoto, R. Xiang, H. An, B. Wang, T. Inoue, S. Chiashi, Y. Ikuhara, S. Maruyama, Synthesis of subnanometer-diameter vertically aligned single-walled carbon nanotubes with copper-anchored cobalt catalysts. *Nanoscale* **8**, 1608–1617 (2016).
30. A. Markström, K. Frisk, B. Sundman, A revised thermodynamic description of the Co-W-C system. *J. Phase Equilib. Diffus.* **26**, 152–160 (2005).
31. A. R. Harutyunyan, G. Chen, T. M. Paronyan, E. M. Pigos, O. A. Kuznetsov, K. Hewaparakrama, S. M. Kim, D. Zakharov, E. A. Stach, G. U. Sumanasekera, Preferential growth of single-walled carbon nanotubes with metallic conductivity. *Science* **326**, 116–120 (2009).
32. D. Q. Zhang, J. Yang, F. Yang, R. Li, M. Li, D. Ji, Y. Li, (*n*,*m*) Assignments and quantification for single-walled carbon nanotubes on SiO_2/Si substrates by resonant Raman spectroscopy. *Nanoscale* **7**, 10719–10727 (2015).
33. F. Hosokawa, T. Shinkawa, Y. Arai, T. Sannomiya, Benchmark test of accelerated multi-slice simulation by GPGPU. *Ultramicroscopy* **158**, 56–64 (2015).
34. F. Hosokawa, H. Sawada, T. Shinkawa, T. Sannomiya, Image transfer with spatial coherence for aberration corrected transmission electron microscopes. *Ultramicroscopy* **167**, 11–20 (2016).

Acknowledgments: We thank T. Ito and H. Tsunakawa for TEM assistance. H.A. thanks the China Scholarship Council for financial support. A.K. acknowledges support from the Leading Initiative for Excellent Young Researchers of MEXT. **Funding:** Part of this work was financially supported by JSPS KAKENHI grant numbers JP18H05329, JP25107002, JP15H05760, and JP15K17984 and IRENA Project by JST-EC DG RTD, Strategic International Collaborative Research Program (SICORP). Part of this work was based on results obtained from a project commissioned by the New Energy and Industrial Technology Development Organization (NEDO) and by the "Nanotechnology Platform" (project no. 12024046) of the Ministry of Education, Culture, Sports, Science and Technology (MEXT), Japan. **Author contributions:** S.M. and R.X. designed the experiment. H.A. performed the catalyst preparation, SWCNT growth, and chirality characterization. R.X. estimated the charge distribution. H.A. and R.X. took the SAED patterns. A.K. and R.X. carried out the TEM/STEM imaging. H.A., C.B., and A.L. performed the structure analysis. A.K. simulated the STEM images and performed the EDS mapping. R.X., A.K., and H.A. wrote the paper. All authors joined the discussion and interpretation of the results. **Competing interests:** The authors declare that they have no competing interests. **Data and materials availability:** All data needed to evaluate the conclusions in the paper are present in the paper and/or the Supplementary Materials. Additional data related to this paper may be requested from the authors.

Submitted 30 September 2018
Accepted 15 April 2019
Published 24 May 2019
10.1126/sciadv.aat9459

Citation: H. An, A. Kumamoto, R. Xiang, T. Inoue, K. Otsuka, S. Chiashi, C. Bichara, A. Loiseau, Y. Li, Y. Ikuhara, S. Maruyama, Atomic-scale structural identification and evolution of Co-W-C ternary SWCNT catalytic nanoparticles: High-resolution STEM imaging on SiO_2. *Sci. Adv.* **5**, eaat9459 (2019).

Atomic-scale structural identification and evolution of Co-W-C ternary SWCNT catalytic nanoparticles: High-resolution STEM imaging on SiO_2

Hua An, Akihito Kumamoto, Rong Xiang, Taiki Inoue, Keigo Otsuka, Shohei Chiashi, Christophe Bichara, Annick Loiseau, Yan Li, Yuichi Ikuhara and Shigeo Maruyama

Sci Adv **5** (5), eaat9459.
DOI: 10.1126/sciadv.aat9459